Article

An Acridone Derivate Simultaneously Featuring Multiple Functions and Its Applications

Yaokun Xia, Wenhui He, Juan Li, Lupeng Zeng, Tingting Chen, Yijuan Liao, Wei-Ming Sun, Jianming Lan, Shuangmu Zhuo, Jing Zhang, HuangHao Yang, and Jing-Hua Chen

Anal. Chem., **Just Accepted Manuscript** • DOI: 10.1021/acs.analchem.9b01289 • Publication Date (Web): 28 May 2019

An Acridone Derivate Simultaneously Featuring Multiple Functions and Its Applications

Yaokun Xia†, Wenhui He†, Juan Li‡, Lupeng Zeng†, Tingting Chen†, Yijuan Liao§, Weiming Sun†, Jianming Lan†, Shuangmu Zhuo//, Jing Zhang*§, Huanghao Yang*‡, Jinghua Chen*†

†Department of Pharmaceutical Analysis, The School of Pharmacy, Fujian Medical University, Fuzhou, Fujian Province 350122 (P. R. China) E-mail: cjh_huaxue@126.com

‡MOE Key Laboratory for Analytical Science of Food Safety and Biology, State Key Laboratory of Photocatalysis on Energy and Environment, College of Chemistry, Fuzhou University, Fuzhou, Fujian Province 350108 (P. R. China) E-mail: hhyang@fzu.edu.cn

§Department of Chemical Biology, College of Life Sciences, Fujian Agriculture and Forestry University, Fuzhou, Fujian Province 350002 (P. R. China) E-mail: 1601225385@qq.com

// Key Laboratory of Optoelectronic Science and Technology for Medicine of Ministry of Education, Fujian Normal University, Fuzhou, Fujian Province 350007 (P. R. China)

ABSTRACT: Compared with plenty of single-functional molecules, multifunctional molecules are scare and have high demand in further research. In this work, a multifunctional molecule called 10-methyl-2-amino-acridone (MAA) is presented. Interestingly, MAA simultaneously featuring electrochemistry, two-photon fluorescence, visible-light-induced oxidase mimic, and photoelectrochemistry (PEC) activity, and the related properties are studied in detailed. Multiple functions integrated into one molecule allows MAA to become a versatile signal probe. Therefore, the MAA is acted as electrochemical indicator to detect exosomal total protein with high sensitivity at first. In addition, MAA is used to one- or two-photon fluorescence imaging *in vitro* and *in vivo*, including cells, 3D tumor spheroids, zebrafish, and exosomes. The results suggest that MAA not only possesses favorable photostability, but it is also suitable for imaging in deep tissue. Furthermore, the visible-light-induced oxidase mimic and photoelectrochemical activities of MAA is selectively inhibited by Cu^{2+}, and the relevant mechanism is carefully analyzed. Based on this phenomenon, we develop a dual-modal detection strategy for detection of Cu^{2+} in river water. Compared with single signal readout model, this strategy is able to avoid false positive and negative detection through two series of data mutually validating each other. Therefore, our study shows that the "multiple-in-one" MAA provides a blueprint for the investigation and application of multifunctional organic molecule.

Introduction

Development of multifunctional probes is of great significance for sensors, biolabeling and other applications.[1] For example, multifunctional probes are often employed to construct multiple modal sensing assay, and produce diverse signal to realize more sensitive and efficient analysis.[2] But most of multifunctional probes are constructed by combining different components together, which suffers the complicated preparation process with high cost.[3,4] Although emergence of some nanomaterials and organic molecules realizes different functions integrate into one component, their tedious structure and synthesis route as well as low thermal and chemical stability restrict their applications.[5-7] In recent years, synthesis of acridone derivates (ADs) is expected to develop a multifunctional molecule, because of its structure simple, modification flexibility and specificity that is extended conjugated plane and electron donor-acceptor system.[8-10] Despite various ADs have been synthesized that supported by previous our works and other groups,[11-13] several key issues still need to be addressed to synthesize ADs with excellent properties. (1) As electrochemical indictor, the related researches about ADs are restricted by poor solubility and electrode types.[14-16] (2) The short excitation wavelength of a proportion of ADs may lead to photodamage, biological autofluorescence, photobleaching and shallow penetration depth.[17,18] (3) The most important is that up till now the multifunctions in the same ADs is still rarely reported. Considering acridone structure is very special, containing an electron-accepting group (C=O) along with an electron-donating nitrogen atom bearing a lone electron pair in acridone moiety and structure modification flexibility,[9,10] it is possible to introduce appropriate groups in acridone, which not only has potential to optimize its electrochemical and fluorescent performance but also may integrate different functions in single compound to enrich multifunctional organic molecule. Therefore, significant effort should be further invested in improving performance and exploring more functions of ADs.

Herein, we present the synthesis of an acridone derivate with methyl and amino modification called MAA. With a simple synthetic method, the modified MAA obtained the following fascinating properties, some of which in ADs were even barely reported. (1) MAA exhibits good water solubility and low toxicity. (2) The electrochemical activity of MAA is measured on different electrodes, including gold electrode (GE), glass carbon electrode (GCE), and indium tin oxide (ITO) electrode. Meanwhile, the reaction between MAA and biomacromolecule such as protein is validated, which is potential to develop a convenient sensing approach with label-free pattern. (3) Based on large π-conjugated system and electron donors ($-CH_3$ and $-NH_2$), the relatively high fluorescence quantum yield, long lifetimes, high photostability, long emission wavelength, and large stokes shift prevent self-quenching effect and reduce the interference from excitation.[19] In addition, the small molecular weight of MAA, enables easy penetration of cell membranes for live cell staining processes.[20] (4) Conjugating electron donating ($-CH_3$ and $-NH_2$) and accepting (C=O) substituents through π-bridges (-π-), the bright two-photon fluorescence of MAA is observed at 810 nm excitation that so called biological optical window, which is able to eliminate the biological autofluorescence, reduce photodamage, and increase

tissue penetration depth.[21,22] As far as we know, the two-photon fluorescence property of ADs is rarely explored. (5) It is interesting that MAA is found to possess effective visible-light-induced oxidase mimic activity, catalyzing 3,3',5,5'-tetramethylbenzydine (TMB) from colorless to blue under xenon lamp, which discards relative harsh reaction conditions because of absence of destructive hydrogen peroxide. Taken together, the vast potential of MAA as multifunctional signal probe is explored in this work.

Experimental Section

Reagents and apparatus. All chemicals were obtained from commercial suppliers and used without further purification. Acridone (AR, 98%) was obtained from MACKLIN Reagent Company. CD63 antibody, AGO_2 antibody, TSG 101 antibody, and EpCAM antibody were provided from Abcam. The HeLa and HepG2 cells were purchased from China Center for Type Culture Collection in Shanghai. Pierce bicinchoninic acid (BCA) Protein Assay Kit and enhanced chemiluminescence reagent were purchased from Thermo Fisher Scientific. 3-(4,5-dimethylthiazol-2-yl)-2,5-diphenyltetrazolium bromide (MTT) were obtained from Aladdin Reagent Co. Ltd. (Shanghai, China). Phosphate buffered saline (PBS), fetal bovine serum (FBS) and roswell park memorial institute (RPMI) were purchased from Hyclone. Hochest 33342 was purchased from Nanjing Kaiji Biological Technology Development Co. Ltd. 1,1'-Dioctadecyl-3,3,3',3'-Tetramethylindocarbocyanine (DiI) was purchased from Beyotime. Zebrafish, culture fluid, and melanin inhibitor were provided from Nanjing one tree pear flower Biotechnology Co. Ltd.. 3,3',5,5'-tetramethylbenzidine (TMB) was purchased from Tokyo Chemical Industry (TCI, Shanghai). All other chemicals were analytical grade. All aqueous solutions were prepared using ultra-pure water (18.2 MΩ, Milli-Q, Millipore). Electrochemical signals were measured by Electrochemical analyzer (CHI 660E, Shanghai Chen Hua Instrument Co. Ltd., China). The ultracentrifuge was Beckman optima XPN-100 (U.S.A.). The transmission electron microscopy (TEM) images were carried out on a JEM-2010 microscope (JEOL Ltd., Japan). The fluorescence spectra were carried out using a fluorescence spectrometer (F-4600, HITACHI, Japan). The UV-Vis absorption spectra were recorded on UV-Vis spectrometer (2450, SHIMADZU, Japan). The separation and purification of MAA was carried out using preparative high performance liquid chromatography (LC-20AP, SHIMADZU, Japan). The one- and two-photon fluorescence imaging of HeLa cells, zebrafish and exosomes were conducted on a confocal fluorescence microscopy (Zeiss, LSM880, Germany).

Preparation of MAA. The synthesis route of MAA was displayed in Figure S1 following previous published procedure with some modifications.[23] Firstly, the compound 1 (10-methyl-acridone) was synthesized through substitute reaction. An amount of 0.4811 g 9(10H)-acridone was put into ethanol and potassium hydroxide mixture, and the temperature was risen to 110-140 ℃. Then, 20 mL N,N-Dimethylformamide and 10 g iodomethane were added into above system, and heated at 165 ℃ for 40 min. The solution was poured into ice water and the yellowish green solid precipitate appeared. The solid was filtered off, washed with 10 mL water and further purified by recrystallization in absolute alcohol. The solid was oven dried at 70 ℃, and the compound 1 was obtained. MS (EI) ($[M+H]^+$)=210.

After that, 0.2105 g compound 1 was dissolved in 6 mL acetic acid, and then added into 2 mL concentrated nitric acid and 2 mL acetic acid, and heated at 58-62 ℃ for 2 h. The solution was poured into ice water, and the golden solid was appeared. The solid was filtered off, washed, and oven dried. The compound 2 (10-methyl-2-nitro-acridone) was obtained. MS (EI) ($[M+H]^+$)=255. Next, the MAA was prepared as following procedures: (1) The 0.1 g compound 2, 2.5 mL Na_2S (30 wt%) and 5 mL ethanol were mixed and added into a round bottom flask, and add into water to 50 mL. The mixture was heated at 130 ℃ under N_2 for 4 h. (2) The obtained solution was poured into ice water, and the solid precipitate was acquired through centrifugation. Then the precipitate was dried in vacuum drying box. (3) Finally, the precipitate was separated and purified by preparative HPLC method with gradient elution to obtain high pure MAA. The conditions of preparative HPLC method were as follows: chromatographic column was C_{18}, mobile phases were acetonitrile and double distilled water, and the flow rate was 2 mL/min, and the column temperature was 35℃. FAB-MS: m/z 225 ($[M+H]^+$); ^{1}H-NMR (400 MHz, $CDCl_3$) δ: 8.572 (d, ArH), 7.841 (s, ArH), 7.718 (t, ArH), 7.514 (d, ArH), 7.443 (d, ArH), 7.261 ($CDCl_3$), 7.202 (d, ArH), 3.887 (s, NH_2), 1.595 (s, CH_3); ^{13}C-NMR (400 MHz, DMSO-d6): δ: 177.65 (-C=O), 142.21 (=C-N), 140.89 (=C-NH_2), 136.37 (=C-N), 133.40 (=CH-), 127.86 (=CH-), 123.59 (=C-C=O), 123.43 (=C-C=O), 121.73 (=CH-), 120.54 (=CH-), 116.05 (=CH-), 114.46 (=CH-), 110.67 (=CH-), 33.55 (-N-CH_3).

Cells culture and exosomes isolation. HepG2 cells were cultured in DMEM containing 10 % FBS and 1 % penicillin-streptomycin, and maintained in a humidified atmosphere of 5 % CO_2 at 37 ℃. Before exosomes isolation, HepG2 cells (1×10^8 cells) were cultured in DMEM containing 5 % FBS (exosomes depleted) for 48 h. Subsequently, the culture supernatant was collected and centrifuged according to previous reported protocol.[24] Briefly, the obtained cell culture supernatant was centrifuged at 300 g for 10 min, 2,000 g for 20 min, and 11,000 g for 45 min to deplete intact cells, cell debris, and protein, respectively. The supernatant then was centrifuged at 110,000 g for 70 min, and the transparent sediment was exosomes. Finally, the exosomes were resuspended in sterile PBS and stored at -80 ℃. Additionally, the HeLa cells were cultured under the same conditions.

One- and two-photon cellular imaging. The HeLa cells were seeded on glass coverslips and incubated at 37 ℃ for 24 h. Then the HeLa cells first were stained with Hochest 33342 (1 μM) for 15 min. Next, the cells were incubated with MAA (20 μM) for 4 h. After every staining, the media was removed, and the cells were washed with PBS (pH 7.4) for three times to remove the unbound dye. After that, the cells were imaged on a Zeiss LSM880 confocal microscope. The fluorescence of Hoechst 33342 and MAA were excited at 405 nm (blue channel) and 488 nm (green channel), respectively. The excitation wavelength of the laser was 810 nm for two-photon imaging. The three-dimensional multicellular spheroid (3DMTS) was constructed according to previous literatures with some modifications.[25,26] The 6.0 mL RPMI containing 90 mg agarose was microwaved until agarose dissolution. The 50 μL of the hot agarose solution was added into each well rapidly and allowed to cool for 30 min. Next, the HeLa cells were seeded in above 96-well plates at 6000 cells per well and were incubated under 5 % CO_2 at 37 ℃ for 72 h. After that, the resulting 3DMTS were incubated with MAA for certain time. Then, the 3DMTS was washed by PBS for three times. Finally, confocal microscopy was used for the spheroids imaging.

One- and two-photon zebrafish imaging. The zebrafishes were maintained in culture solution containing 2 % melanin inhibitor at room temperature for 2 days. 10 μM MAA was incubated with zebrafishes at room temperature for 12 h. Finally, the MAA labeled zebrafishes were imaged by Zeiss LSM880 confocal fluorescence microscope for one-photon and two-photon fluorescence imaging after washing by zebrafishes culture fluid for three times to remove the free MAA.

One- and two-photon exosomes imaging. The HepG2 cells derived exosomes were treated with 10 μM MAA in PBS (pH 6.8) for 30 min at room temperature. After washing three times by

PBS, the MAA labeled exosomes were obtained. The exosomes fluorescence imaging procedure as following: (1) the HepG2 cells were stained by Hochest 33342 (1 μM) for 15 min and washed by PBS for three times. (2) The aforementioned cells were incubated with MAA labeled exosomes for 1 h, followed by washing with PBS for three times. (3) The one-photon fluorescence imaging was measured by Zeiss LSM880 confocal fluorescence microscope. The fluorescence of Hoechst 33342 and MAA were excited at 405 nm (blue channel) and 488 nm (green channel), respectively. As for two-photon fluorescence imaging, the images were obtained by Zeiss LSM880 confocal fluorescence microscope with excitation of 810 nm. For fluorescence co-localization analysis, the MAA-labeled exosomes were incubated with DiI for 30 min to acquire MAA and DiI dual-labeled exosomes. The DiI was excited by using laser at 561 nm.

Cu^{2+} detection by use of MAA as oxidase mimicking. The Cu^{2+} detection was based on color change of TMB. In a typical experiment, 10 μM of MAA was incubated with different concentration Cu^{2+} for a certain time in pH 4.0 HAc-NaAc buffer solution (10 mM) at room temperature. Following that, 500 μM TMB was added in the above solution and illuminated for 5 min under visible light (λ≥400 nm). Finally, 2 μL of 2 M H_2SO_4 was added, and the absorbance at 450 nm was measured by a UV-Vis spectrophotometer.

Cu^{2+} detection by photoelectrochemistry. Detection of Cu^{2+} was carried out as follows: the ITO electrode was modified with MAA before detection firstly. Subsequently, the ITO electrode was immersed in a NaAc-HAc buffer solution (10 mM, pH 4.0) with different concentration Cu^{2+} to measure the photocurrent signal.

Electron spin resonance (ESR). 10 μM MAA and 100 mM spin trap 5,5-dimethyl-1-pyrroline N-oxide (DMPO) in anhydrous methanol solution were photoirradiated with visible light for 0, 5 or 10 min, respectively. Subsequently, the prepared samples were transferred to a quartz capillary tube and placed in the ESR cavity, and obtained the ESR spectra using a JES FA 200 ESR spectrometer (JEOL, Japan).

Results and discussion

Synthesis and characterization of MAA. The synthesis of MAA is accomplished as described in Figure S1 with substituent and reduction reaction: Firstly, link a methyl and a nitro to the 2, 10-positions of acridone, respectively.[14] Subsequently, the nitro is reduced to amino by Na_2S, and the crude product is purified by preparative HPLC to obtain pure MAA. The relevant characterization data are provided in Figure S2~Figure S4. Moreover, the color of MAA and water solubility exhibit obvious change comparing with acridone and other intermediates (Figure S5). Above results suggest that MAA is synthesized successfully.

Electrochemical properties and detection of exosomal total protein. The electrochemical activity of MAA is studied on different electrodes firstly. A couple of redox peaks of MAA are acquired on different electrodes (Figure S6A) compared to acridone (Figure S6B). The peak current of MAA is proportional to the square root of scan rate, indicating a diffusion-controlled process (Figure S7A and Figure S7B). The effect of pH on formal potential and peak current of MAA suggests protons participate in the electrode process (Figure S7C and Figure S7D), and the electron transfer number is equal to proton number. The relevant details are exhibited in section 1 (Supporting Information). Moreover, the MAA also can bind with biomacromolecule, such as protein, to induce electrochemical signal change. The result indicates the forming of a 1:1 association between MAA and BSA (Figure S8), and the interaction mechanism and binding ratio are showed in section 2 (Supporting Information). Based on the described properties, we thereupon envisage that MAA is acted as an electrochemical indicator for protein concentration analysis because of the inherent high sensitivity of electrochemistry comparing with BCA protein assay that is a classic protein analysis method. Figure S9A illustrates that the linear relationship is obtained between ΔI_p and the concentration of BSA. As a demonstration, our method is applied to the determination of the total protein in exosomes solution. Exosomes are membrane-enclosed vesicles secreted by various cells, and they carry abundant molecular information of their parent cells such as protein.[27] The exosomal protein concentration is higher in advanced-stage disease, so they have been revealed as a promising biomarker for liquid biopsy.[28] Before analysis content of exosomal protein, the exosomes are characterized according to International Society for Extracellular Vesicles (ISEV) guidelines.[29] At first, a mean diameter of exosomes measured by dynamic light scattering (DLS) is about 130 nm (Figure 1A). The morphologies of exosomes are characterized by transmission electron microscope (TEM) (Figure 1A, inset), exhibiting saucer like, and the average diameter shows ~100 nm that smaller than that detected by DLS, which is ascribed to shrink of exosomes during the preparation process for TEM.[30] The western blot (WB) images for different categories proteins validate the efficiency of the separation of exosomes (Figure 1B). Figure S9B shows the exosomal total protein concentration that acquired by our method is closed to that of the traditional BCA method. The t-test is utilized to quantitatively analyze if two series of data from electrochemistry and BCA are significantly different from each other. The P-value is 0.517, much larger than 0.05, indicating that there is no significant difference between two results, so this strategy is reliable in practical application. Taken together, this approach is prospective in generating label-free pattern for detecting other proteins selectively coupling with aptamer technology that is similar to previous work.[31]

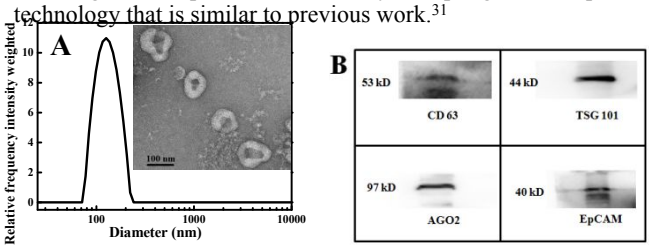

Figure 1. (A) The size distribution of exosomes analyzed by DLS, inset: The TEM image of exosomes. (B) WB images in exosomes for CD 63, TSG 101, AGO_2 and EpCAM.

Optical properties and fluorescence imaging in cells, 3D tumor spheroids, zebrafish, and exosomes. The optical properties are explored in detailed. Because of electron-donating effect of methyl and amino, UV-Vis absorbance peaks of MAA are red-shifted from ~250 nm to ~260 nm and ~390 nm to ~420 nm, respectively (Figure S10A), and optimal fluorescence emission wavelength is located at 540 nm (Figure S10B), exhibiting strong green fluorescence (Figure S10B, inset). Compared with acridone (Δλ=40 nm, Figure 2A), MAA has a three-fold increase of Stoke shift (Δλ=120 nm, Figure 2B), which is promising to achieve precise imaging and accurate sensing. The absolute fluorescence quantum yields and lifetime are 12.3 % and 461.82 ns, respectively, which is superior to acridone (Table S1). Especially, the long fluorescence lifetime of MAA may provide a neat opportunity for fluorescence lifetime imaging in future.[32] Surprisingly, two-photon fluorescence of MAA is found in our work (Figure 2C). The slop of double logarithm plot between fluorescence intensity and laser power remains at 2 (Figure 2D), indicative of quadratic dependence, illustrating it is a two-photon excitation process.[33] Thus, MAA is potential to act as probe for fluorescence imaging.

The low toxicity is precondition for bioimaging. As shown in Figure S11, high viability is obtained after the cells being

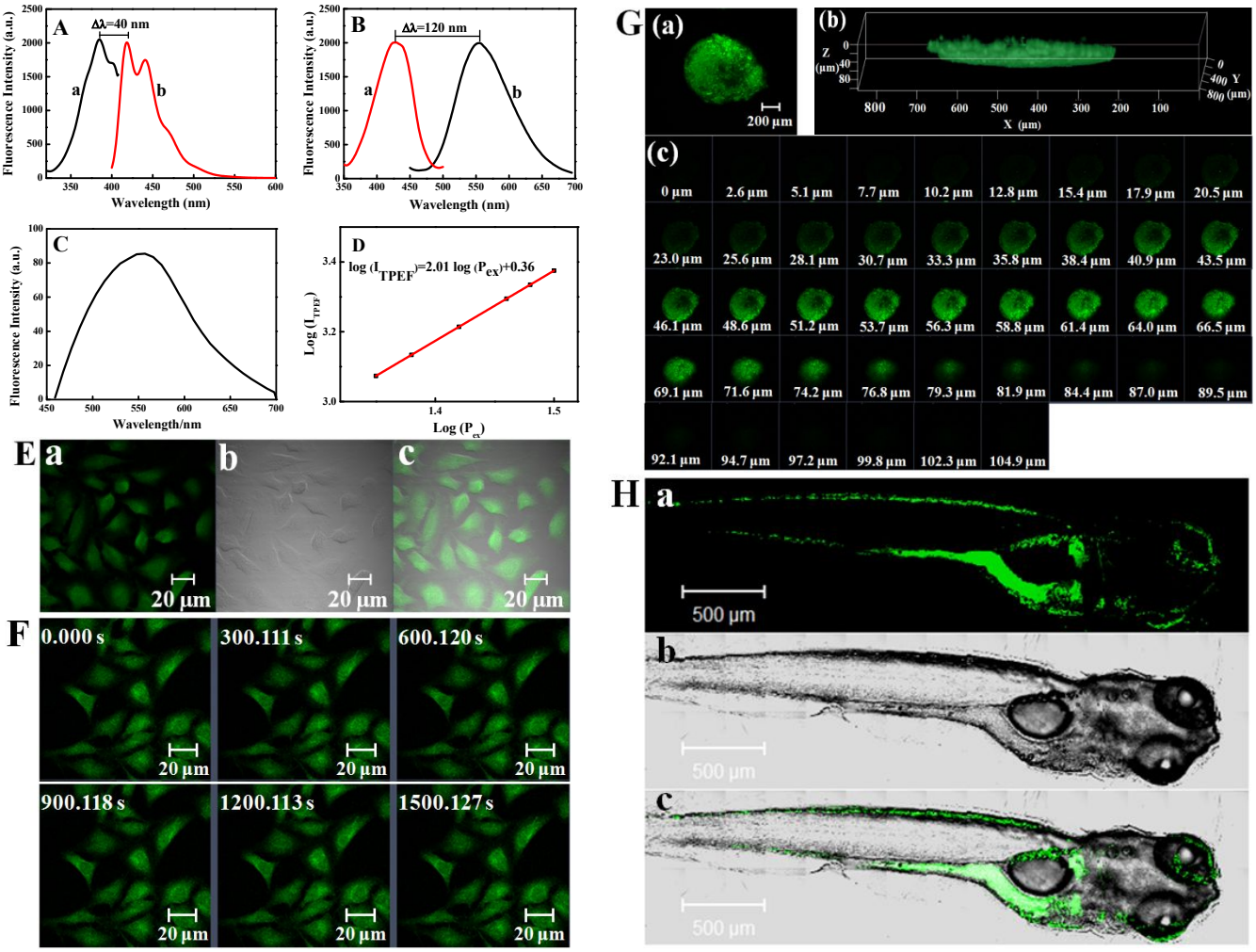

Figure 2. (A) The excitation (a) and emission (b) spectrum of acridone. (B) The excitation (a) and emission (b) spectrum of MAA. (C) Two-photon fluorescence spectrum of MAA with femtosecond pulsed laser. (D) Double logarithmic plots of between two-photon fluorescence intensity and laser power. (E) Two-photon microscopy images of HeLa cells incubated with MAA (a), bright field image of HeLa cells (b), overlay image of a and b (c). (F) Two-photon confocal images of MAA for photobleaching in HeLa cells. (G) Two-photon microscopy images of 3D tumor spheroids (a), the two-photon 3D Z-stack images of an intact spheroid (b), the two-photon Z-stack images were taken from the top to bottom (c). (H) Two-photon microscopy images of living zebrafish incubated with MAA (a), bright field image of zebrafish (b), overlay image of a and b (c).

incubated with 20 μM MAA even for 20 h, which indicates that MAA presents hypotoxicity under the cell imaging conditions. To investigate the fluorescence imaging feasibility of MAA *in vitro*, the uptake of MAA by HeLa cells is conducted. One- (Figure S12) and two-photon (Figure 2E) fluorescence microscopy images illustrate that MAA penetrates cell membrane efficiently. To understand the distribution of MAA in cell, HeLa cells are incubated with nuclear dye Hoechest 33342 and MAA. The nuclei of HeLa cells stained Hoechest 33342 shows a blue color (Figure S12B). The green emission from MAA full of whole cell (Figure S12C and Figure S12D), indicating the MAA not only gets into the cytoplasm, but also enters the nuclei. Besides, photobleaching experiment is conducted in HeLa cells due to photostability being an important parameter for long-term biological imaging. Figure S13 and Figure 2F display the fluorescence intensities with one- or two-photon excitation for 1500 s are still changed minimally, and quantitative photobleaching results (Figure S14) show MAA possesses superior photostability than other fluorescent probes that reported by previous literatures.[25,34-38] Furthermore, the imaging depth is the other important parameter for fluorescence imaging because it is conducive to noninvasive biological imaging. A tissue penetration depth experiment using 3DMTSs as model is investigated. The fluorescence intensity is obtained from 3DMTS only 58.8 μm for the one-photon excitation (Figure S15). Compared with one-photon excitation, signal is detected even to 104.9 μm for the two-photon excitation (Figure 2G). Additionally,

from the quantification graphs of one-photon (Figure S16A) and two-photon (Figure S16B) fluorescence images for 3DMTS, the deeper penetration of two-photon excitation is observed intuitively, which is ascribed to the low absorption of near-infrared (NIR) light by the biological environment,[39] and enables MAA as an effective two-photon probe for fluorescence imaging to observe physiological condition in deep of tissue.

Currently, fluorescence imaging *in vivo* become a hotspot because of it being an effective avenue to understand the pathological process and drug adsorption, distribution, metabolism, and excretion (ADME).[40] To investigate the application of MAA imaging *in vivo*, the zebrafish is acted as study subject because of its small size, transparent body, rapid maturation, and highly genome homologous with human.[41,42] Before fluorescence imaging, the zebrafish that is incubated with MAA is washed by culture fluid for several times to eliminate non-specific adsorption. From Figure 2H and Figure S17, the zebrafish emits green fluorescence after cultured in MAA solution for 12 h, which illustrates the MAA is introduced into the body. We also observe that MAA is tissue-dependent affinity, and mainly accumulated at the head, abdominal cavity and tail (Figure 2H). MAA is accumulated at eyes, but the eyeball is dark, which demonstrates that the MAA not enters across the blood-ocular barrier. The abdominal cavity is the brightest part of the body and indicates that MAA enters into the digestive system, revealing that swallowing is a primary avenue for MAA entering into zebrafish. The brightness of the dorsal aorta illustrates that MAA enters into the circulatory system, which is important for MAA transportation in zebrafish body. In brief, MAA is a potential fluorescent probe for *in vivo* imaging, and above results from zebrafish possess a certain reference value for other animal models owing to zebrafish having high homology with mammals.

Furthermore, recent evidence indicates that exosomes play an important role in transfer of informative molecules between neighboring or even distant cells.[43] Notably, it is difficult to understand the distribution of exosomes in cell due to lack of effective imaging probe. Thus, the development of a proper probe for clear visualization of exosomes is highly desirable. Before exosomes imaging experiment, the recipient cell nuclei are stained by Hoechest 33342 and display blue fluorescence (Figure S18B). The MAA labeled exosomes exhibiting green fluorescence, and located at cytoplasm (Figure S18C and D). To further validate exosomes being imaged in cell, we utilized DiI, a fluorescence dye commonly used for staining exosomes,[44,45] to label exosomes and study exosomes internalization by cells. The cell nuclei showed blue fluorescence (Figure S19A). After the MAA and DiI dual-labeled exosomes were cultured with HepG2 cells for a certain time, the green and red fluorescence in cytoplasm are observed (Figure S19B and S19C). In addition, the orange fluorescence is emergence (Figure S19D), which suggests that the MAA green fluorescence is co-localized with the red fluorescence of DiI. All these results indicate that exosomes are uptake by cells and imaged indeed, which was similar with previous reports.[46,47] Equally, the MAA labeled exosomes are visualization under two-photon fluorescence microscopy (Figure S18E, F and G). So we have realized the one- and two-photon fluorescence imaging for exosomes, and provide a new way for tracking of exosomes *in vitro*. Compared to existing strategies for labelling exosomes, our conjugation-free labelling strategies without complex pretreatment, chemical modification or engineering for exosomes is time- and labor- saving, and user- and bio-friendly.[48-50]

Visible-light-induced oxidase mimic and photoelectrochemistry activities. Besides above properties, the visible-light-induced oxidase-mimicking activity of MAA is found. As far as we know, the visible-light-induced oxidase mimic is rarely reported in acridone derivate. Under visible light irradiation, MAA is able to catalyze the oxidation of different substrates including TMB (Figure S20A), 2,2'-Azinobis-(3-ethylbenzothiazoline-6-sulphonate) (ABTS) (Figure S20B) and o-Phenylenediamine (OPD) (Figure S20C). It is noted that MAA shows catalytic activity under mild reaction conditions without the use of destructive H_2O_2 and the catalytic reaction is controllable just regulating light irradiation time simply. In order to elucidate the reactive species in this catalytic reaction induced by visible light, different scavengers for related reactive species

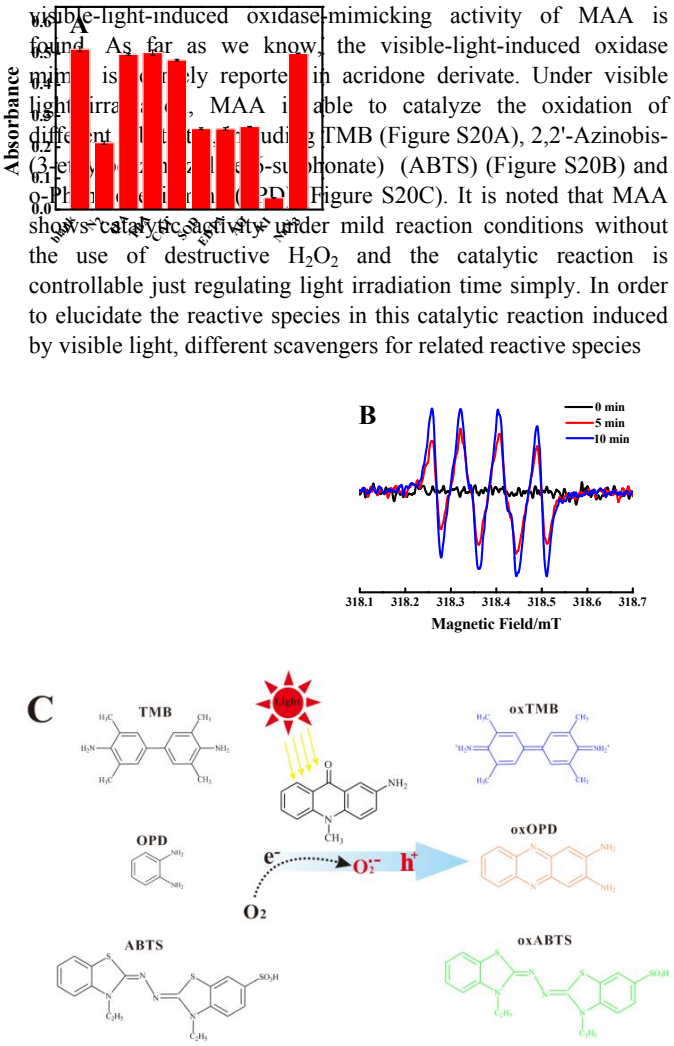

Figure. 3 (A) Effects of scavengers on the TMB-MAA chromogenic reaction under visible light irradiation. (B) The ESR spectra of MAA with spin trap DMPO after irradiation with visible for different time. (C) Proposed mechanism for visible light stimulated oxidase mimic activity of MAA.

such as hydroxyl radicals (·OH), singlet oxygen ($^1O_2$), superoxide anions ($O_2^{\bullet-}$) and photo-genetrated holes (h^+) are added to the system. From Figure 3A, the absorbance of oxidized TMB (oxTMB) has almost no change after reacting with ·OH scavenger isopropanol (IPA) or tert-butanol (TBA), which demonstrates that ·OH is not mainly reactive species. Similarly, the photocatalytic activity is not affected in the presence of NaN_3, which is employed to scavenge $^1O_2$. It shows that $^1O_2$ is not the main reactive oxygen species. As an efficient enzyme for decomposing of H_2O_2 to H_2O and O_2, catalase (CAT) can not affect the absorbance of oxTMB, which indicates that H_2O_2 is not produced during the illumination process. In contrast, the absorbance dramatically decreased after adding h^+ scavengers such as EDTA, ammonium oxalate (AO) or KI, demonstrating that h^+ is one of a reactive specie during the catalytic process. The absorbance of oxTMB obviously decrease after the reaction system purged by N_2, showing the dissolved oxygen plays a key role in the photocatalytic reaction. The catalytic activity is also suppressed in the presence of superoxide dismutase (SOD) that a $O_2^{\bullet-}$ scavenger, indicating $O_2^{\bullet-}$ is a crucial specie. Electron spin resonance (ESR) spectroscopy provides direct evidence to validate that MAA generates $O_2^{\bullet-}$ under visible light irradiation and the quantity of $O_2^{\bullet-}$ depends on the illumination time (Figure 3B). When MAA is irradiated by visible light, it generates electrons in the lowest unoccupied molecular orbital (LUMO) and leaves h^+ in highest occupied molecular orbital (HOMO) to react with TMB. The produced electrons may be trapped by dissolved oxygen to form

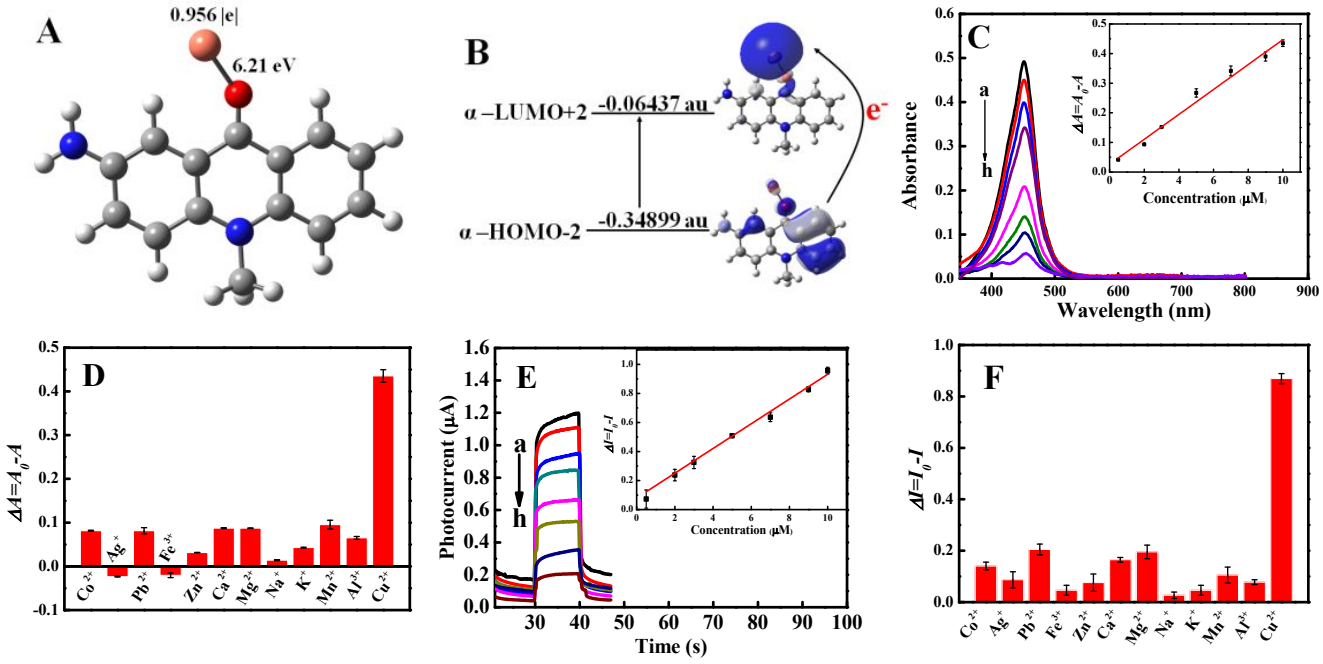

Figure. 4 (A) Structural sketch map of MAA-Cu. (B) Transition orbitals involved in the crucial excited state. (C) UV-Vis response to different concentration Cu^{2+} (from a to h: 0, 0.5, 2, 3, 5, 7, 9, 10 μM), the inset shows corresponding calibration curve (D) Selectivity of the UV-Vis toward Cu^{2+} and different metal ions. (E) photocurrent response to different concentration Cu^{2+} (from a to h: 0, 0.5, 2, 3, 5, 7, 9, 10 μM), the inset shows corresponding calibration curve. (F) Selectivity of the PEC toward Cu^{2+} and different metal ions.

$O_2^{\bullet-}$ radicals that also can oxidize TMB. Moreover, the PEC is conducted to verify the photoinduced charge transfer of MAA in this system. A reproducible photocurrent response to light irradiation on/off cycles is observed (Figure S21), which indicates there are charge generation, separation, and transfer process. Based on above results, the mechanism of substrates oxidation by photoactivated MAA is shown in Figure 3C. The Michaelis-Menten (Km) constant obtained (Table S2) from Michaelis-menten equation of MAA (Figure S22) is lower than that of fluorescein and 2-aminoacridone (2-AA) as visible light induced oxidase mimic, indicating that it has higher affinity to TMB. The catalytic constant (Kcat) and catalytic efficiency (Kcat/Km) of

MAA are superior to 2-AA (Table S2), which is ascribed to the larger binding energy between MAA and TMB through molecular simulation (Figure S23). Although the Kcat and Kcat/Km of MAA are lower than fluorescein to date (Table S2),[51] which maybe improved significantly through introducing appropriate groups based on its structure modification flexibility.

Detection of Cu^{2+}. Quite impressively, we find that the visible-light-induced oxidase mimicking activity and photocurrent of MAA is selectively inhibited by Cu^{2+}. Molecular simulation is used to understand the mechanism about this phenomenon. The density functional theory (DFT) computation indicates that Cu^{2+} and TMB are both inclined to bind with carbonyl group of MAA in solution (Figure 4A and Figure S23A). Note that the binding energy between Cu^{2+} and MAA is as large as 6.21 eV, which is greatly larger than that (0.20 eV) between TMB and MAA. Considering the stronger interaction between Cu^{2+} and MAA, the carbonyl group of MAA will be occupied by Cu^{2+} rather than TMB, leading to the weakened catalytic efficiency. Besides, the time-dependent DFT (TD-DFT) calculation reveals that an obvious electron transfer from the π orbital of MAA to the 4s orbital of Cu^{2+} occurs in the MAA-Cu compound (Figure 4B), which is further confirmed by the natural bond orbital (NBO) charge (0.956 |e|) on Cu atom (Figure 4A). Such an electron transfer can justify the decrease of photocurrent (Figure S21) and ESR (Figure S24) response in presence of Cu^{2+}. Because Cu^{2+} is harmful to liver and kidneys if short-time exposure to high-level of Cu^{2+},[52] an analysis platform based on MAA could be put forward for Cu^{2+} detection. Before the detection of Cu^{2+}, some important conditions were investigated. As shown in Figure S25, pH 4.0 was chosen for further study (Figure S25A), 5 min was the optimal irradiation time (Figure S25B). Thus, under optimal conditions, along with the increase of Cu^{2+} concentration, the UV-Vis absorbance is decreased (Figure 4C). As expected, the difference in color of solution is significant with the change of Cu^{2+} concentration, which is observed directly by naked eyes (Figure S26). A highly linear relationship between Cu^{2+} concentration and absorbance at 450 nm is observed in the range of 0.5 μM to 10 μM. The correlation equation could be expressed as ΔA=0.042C+0.0263 (r=0.9912), where the ΔA is defined as A_0-A (A_0 and A are the absorbance at 450 nm in the absence and presence of Cu^{2+}, respectively) (Figure 4C, inset). The detection of limit (LOD) of 0.36 μM is based on 3σ method. In addition, this method exhibits good ability to resist interference from common metal ions (Figure 4D). It is worthy noting that the ΔA of Ag^{+} and Fe^{3+} was negative, which indicates these metal ions could oxidized TMB directly. This phenomenon is reported by previous literature.[53,54] However, the ΔA of Ag^{+} and Fe^{3+} is relatively low, which is not able to influence the selectivity of this method. Meanwhile, the photocurrent is also decreased with Cu^{2+} concentration change (Figure 4E), and ΔI is proportional to Cu^{2+} concentration from 0.5 μM to 10 μM. The correlation equation is ΔI=0.0852C+0.0803 (r=0.9961), where the ΔI was defined as I_0-I (I_0 and I were the photocurrent intensities in the absence and presence of Cu^{2+}, respectively) (Figure 4E, inset). The LOD is 0.17 μM (Figure 4E, inset). Similarly, PEC also shows good selectivity (Figure 4F). The feasibility of this method

Table 1. Detection of Cu^{2+} in river water

sample	Add (μM)	Detection by UV-Vis (μM)	Recovery %	Detection by PEC (μM)	Recovery %
River water 1	2	1.92±0.034	96.0	2.01±0.042	100.5
River water 2	3	3.02±0.053	100.7	2.98±0.061	99.3
River water 3	5	5.03±0.045	100.6	4.96±0.058	99.2
River water 4	7	6.98±0.067	99.7	7.09±0.074	101.3
River water 5	9	9.09±0.093	101.0	8.99±0.096	99.9

for Cu^{2+} detection in river water is validated using standard addition method. From Table 1, the recovery rate ranged from 96.0-101.0 % and 99.2-101.3 % for UV-Vis and PEC, respectively. The P-value from t-test is 0.999, much larger than 0.05, indicating that there is no significant difference between data from colorimetry and PEC. In addition, set the concentration that detected by PEC and UV-Vis as the *x* axis and *y* axis, respectively, a good linear relationship is obtained (Figure 5), which indicates the practicability of this strategy in the spiked river water.[55] Compared with conventional single signal readout model, this work with dual-modal signal readout exhibits a more reliable and accurate result, benefiting from the different mechanism and relatively independent signal transduction.[56]

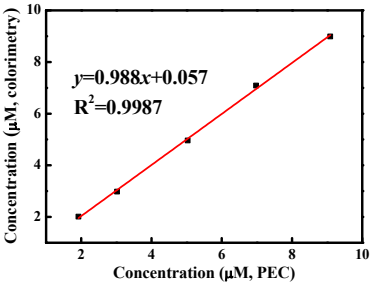

Figure 5. Correlation of the detection results of Cu^{2+} in the recovery test between the developed colorimetric and photoelectrochemical methods.

Conclusion

In summary, we synthesized a smart probe MAA by a facile method and study its multiple properties in details, including electrochemistry, one- and two-photon fluorescence, visible-light-induced oxidase-mimicking, and PEC characteristic. Based on these properties, MAA was employed to act as an electrochemical indicator for exosomal total protein analysis firstly. Then, one- and two-photon fluorescence images in cell, zebrafish, and exosomes were conducted successfully based on the tempting fluorescence property of MAA. Subsequently, we studied the related mechanism about Cu^{2+} inhibiting visible-light-induced oxidase mimic and PEC activities of MAA, and develop a dual-modal strategy for Cu^{2+} detection. Continued research on introducing different groups to further improve the performance of MAA based on its structure modification flexibility. Additionally, we envision building lipsome to encapsulate MAA,[57] it is not only a promising content-release and signal amplification system when bind with target, but also it can realize multiple-modal signal readout in one platform.[58] Consequently, we believe that the multifunctional MAA can be used as an ideal candidate for many chemical and biochemical applications.

ASSOCIATED CONTENT

Supporting Information

This material is available free of charge via the Internet at http://pubs.acs.org. Fluorescence properties of MAA and acridone (Table S1); comparison of catalytic activity (Table S2); the synthesis route; the characterization data; the photograph of solid powder and solution; the CVs of MAA and acridone; the electrochemical properties of MAA; the interaction mechanism between MAA and BSA; detection of exosomal total protein; UV-Vis and fluorescence spectra; cytotoxicity of MAA; one-photon fluorescence images of HeLa cells; photobleaching of MAA; Quantitative photobleaching results for one- and two-photon imaging; one-photon fluorescence images of tumor speroids; quantification graph of one- and two-photon fluorescence images for 3DMTS; one-photon fluorescence images of zebrafish; fluorescence images of exosomes; one-photon fluorescence images of MAA and DiI labelled exosomes; visible-light-induced oxidase mimic of MAA for different substrate; photocurrent of MAA and MAA-Cu; steady-state kinetic analysis; the optimized structures of MAA-TMB and 2-AA-TMB; the ESR spectra of MAA and MAA-Cu; optimization of experimental conditions; photographs of the colorimetric method at different concentrations of Cu^{2+} (Figure S1-S26).

AUTHOR INFORMATION

Corresponding Authors

*E-mail: 1601225385@qq.com (J. Zhang).
*E-mail: hhyang@fzu.edu.cn (H. Yang).
*E-mail: cjh_huaxue@126.com (J. Chen).

Notes

The authors declare no competing financial interest.

ACKNOWLEDGMENT

The authors gratefully acknowledge the National Science Foundation of China (Nos. 21874019, 21635002, 21622502, U1505221, 81771881), the Natural Science Foundation of Fujian Province (Nos. 2017J07001, 2016J05035, 2017J06004, 2018J07004), United Fujian Provincial Health and Education Project for Tacking the Key Research P.R. China (WKJ2016-2-30), the Fujian Science and Technology Innovation Joint Found Project (2016Y9050), Startup Fund for Scientific Research, Fujian Medical University (2017XQ2015).

REFERENCES

(1) Comby, S., Surender, E. M.; Kotova, O.; Truman, L. K.; Molloy, J. K.; Gunnlaugsson, T. *Inorg. Chem.* **2014,** 53, 1867-1879.
(2) Gao, X. X.; Zhou, X.; Ma, Y. F.; Wang, C. P.; Chu, F. X. *New J. Chem.* **2018,** 42, 14751-14756.
(3) Yan, Q.; Ding, X. Y.; Chen, Z. H.; Xue, S. F.; Han, X. Y.; Lin, Z. Y.; Yang, M.; Shi, G.; Zhang, M. *Anal. Chem.* **2018,** 90, 10536-10542.
(4) Zhang, J.; Liang, Y. C.; Lin, X.; Zhu, X.; Yan, L.; Li, S.; Yang, X.; Zhu, G.; Rogach, A. L.; Yu, P. K.; Shi, P.; Tu, L. C.; Chang, C. C.; Zhang, X.; Chen, X.; Zhang, W.; Lee, C. S. *ACS Nano* **2015,** 9, 9741-9756.
(5) Gui, R.; Jin, H.; Wang, Z.; Li, J. *Chem. Soc. Rev.* **2018,** 47, 6795-6823.

(6) Yan, Z.; Wei, G.; Guang, S.; Xu, M.; Ren, X.; Wu, R.; Zhao, G.; Ke, F.; Xu, H. *Dyes Pigments* **2018,** 159, 542-550.
(7) Avirah, R. R.; Jyothish, K.; Ramaiah, D. *Org. Lett.* **2007,** 9, 121-124.
(8) Sharma, B. K.; Shaikh, A. M.; Agarwal, N.; Kamble, R. M. *RSC Adv.* **2016,** 6, 17129-17137.
(9) Wu, H.; Zhang, Z.; Liu, Q.; Liu, T.; Ma, N.; Zhang, G. *Org. Lett.,* **2018,** 20, 2897-2901.
(10) Pander, P.; Swist, A.; Motyka, R.; Soloducho, J.; Dias, F. B.; Data, P. *J. Mater. Chem. C* **2018,** 6, 5434-5443.
(11) Shu, B.; Cao, J.; Kuang, G.; Qiu, J.; Zhang, M.; Zhang, Y.; Wang, M.; Li, X.; Kang, S.; Ou, T. M.; Tan, J. H.; Huang, Z. S.; Li, D. *Chem. Commun.* **2018,** 54, 2036-2039.
(12) Adhikari, S.; Ghosh, A.; Mandal, S.; Sahana, A.; Das, D. *RSC Adv.* **2015,** 5, 33878-33884.
(13) Li, C.; Liu, Z.; Cai, S.; Wen, F.; Wu, D.; Liu, Y.; Wu, F.; Lan, J.; Han, Z.; Chen, J. *Electrochem. Commun.* **2015,** 60, 8340-8343.
(14) Chen, J. H.; Zhang, X.; Cai, S.; Wu, D.; Lin, J.; Li, C.; Zhang, J. *Biosens. Bioelectron.* **2014,** 53, 12-17.
(15) Wang, B.; Bouffier, L.; Demeunynck, M.; Mailley, P.; Roget, A.; Livache, T.; Dumy, P. *Bioelectrochemistry* **2004,** 63, 233-237.
(16) Chen, J.; Zhang, J.; Huang, L.; Lin, X.; Chen, G. *Biosens. Bioelectron.* **2008,** 24, 349-355.
(17) Xia, Y.; Wang, L.; Li, J.; Chen, X.; Lan, J.; Yan, A.; Lei, Y.; Yang, S.; Yang, H.; Chen, J. *Anal. Chem.* 2018, **90,** 8969-8976.
(18) Gao, C.; Zhang, W.; He, S.; Li, S.; Liu, F.; Jiang, Y. *Bioorg. Chem.* **2015,** 60, 30-36.
(19) Ren, T. B.; Xu, W.; Zhang, W.; Zhang, X. X.; Wang, Z. Y.; Xiang, Z.; Yuan, L.; Zhang, X. B. *J. Am. Chem. Soc.* **2018,** 140, 7716-7722.
(20) Mosquera, J.; García, I.; Liz-Marzán, L.M. *Acc. Chem. Res.* **2018,** 51, 2305-2313.
(21) He, G. S.; Tan, L. S.; Zheng, Q.; Prasad, P. N. *Chem. Rev.* **2008,** 108, 1245-1330.
(22) Kim, H. M.; Cho, B. R. *Chem. Rev.* **2015,** 115, 5014-5055.
(23) Hibbard, H. A. J.; Reynolds, M. M. *J. Mater. Chem. B* **2019,** 7, 2009-2018.
(24) Xia, Y.; Liu, M.; Wang, L.; Yan, A.; He, W.; Chen, M.; Lan, J.; Xu, J.; Guan, L.; Chen, J. *Biosens. Bioelectron.* **2017,** 92, 8-15.
(25) Qiu, K.; Huang, H.; Liu, B.; Liu, Y.; Huang, Z.; Chen, Y.; Ji, L.; Chao, H. *ACS Appl. Mater. Interfaces* **2016,** 8, 12702-12710.
(26) Charoen, K. M.; Fallica, B.; Colson, Y. L.; Zaman, M. H.; Grinstaff, M. W. *Biomaterials* **2014,** 35, 2264-2271.
(27) Jiang, Y.; Shi, M.; Liu, Y.; Wan, S.; Cui, C.; Zhang, L.; Tan, W. *Angew. Chem. Int. Ed.* **2017,** 56, 11916-11920.
(28) Cui, S.; Cheng, Z.; Qin, W.; Jiang, L. *Lung Cancer* **2018,** 116, 46-54.
(29) Lötvall, J.; Hill, A. F.; Hochberg, F.; Buzás, E. I.; Vizio, D.; Di Gardiner, C.; Gho, Y. S.; Kurochkin, I. V.; Mathivanan, S.; Quesenberry, P.; Sahoo, S.; Tahara, H.; Wauben, M. H.; Witwer, K. W.; Théry, C. *J. Extracell. Vesicles* **2014,** 3, 26913.
(30) W. Zhang, P. Peng, Y. Kuang, J. Yang, D. Cao, Y. You, K. Shen, *Tumour. Biol.* **2016,** 37, 4213-4221.
(31) Labib, M.; Green, B.; Mohamadi, R. M.; Mepham, A.; Ahmed, S. U.; Mahmoudian, L.; Chang, I. H.; Sargent, E. H.; Kelley, S. O. *J. Am. Chem. Soc.* **2016,** 138, 2476-2479.
(32) Deng, H. H.; Zhang, L. N.; He, S. B.; Liu, A. L.; Li, G. W.; Lin, X. H.; Xia, X. H.; Chen, W. *Biosens. Bioelectron.* **2015,** 65, 397-403.
(33) Deng, F.; Sommer, J. R.; Myahkostupov, M.; Schanze, K. S.; Castellano, F. N. *Chem. Commun.* **2013,** 49, 7406-7408.
(34) Li, D.; Qiu, W.; Xu, B.; Qian, J.; Tang, B. Z. *Adv. Mater.* **2017,** 29, 1703643.
(35) Song, X.; Liu, F.; Sun, S.; Wang, J.; Cui, J.; Peng, X. *RSC Adv.* **2014,** 4, 9326-9329.
(36) Wang, C.; Fukazawa, A.; Taki, M.; Sato, Y.; Higashiyama, T.; Yamaguchi, S. *Angew. Chem. Int. Ed.* **2015,** 54, 15213-15217.
(37) Shimi, T.; Koujin, T.; Segura-Totten, M.; Wilson, K. L.; Haraguchi, T.; Hiraoka, Y. *J. Struct. Biol.* **2014,** 147, 31-41.
(38) Gaur, P.; Kumar, A.; Dey, G.; Kumar, R.; Bhattacharyya, S.; Ghosh, S. *ACS Appl. Mater. Interfaces* **2016,** 8, 10690-10699.
(39) Sun, W.; Fan, J.; Hu, C.; Cao, J.; Zhang, H.; Xiong, X.; Wang, J.; Cui, S.; Sun, S.; Peng, X. *Chem. Commun.* **2013,** 49, 3890-3892.
(40) Kang, Y. F.; Li, Y. H.; Fang, Y. W.; Xu, Y.; Wei, X. M.; Yin, X. B. *Sci. Rep.* **2015,** 5, 11835.
(41) Li, Y.; Chen, T.; Miao, X.; Yi, X.; Wang, X.; Zhao, H.; Lee, S. M.; Zheng, Y. *Pharmacol. Res.* **2017,** 125, 246-257.
(42) Kalueff, A. V.; Stewart, A. M.; Gerlai, R. *Trends Pharmacol. Sci.* **2014,** 35, 63-75.
(43) Liu, L.; Liu, Y.; Feng, C.; Chang, J.; Fu, R.; Wu, T.; Yu, F.; Wang, X.; Xia, L.; Wu, C.; Fang, B. *Biomaterials* **2019,** 192, 523-536.
(44) Zhang, Y. Z.; Liu, F.; Song, C. G.; Cao, X. L.; Zhang, Y. F.; Wu, H. N.; Guo, C. J.; Li, Y. Q.; Zheng, Q. J.; Zheng, M. H.; Han, H. *Biochem. Biophys. Res. Commun.* **2018,** 495, 892-898.
(45) Vandergriff, A.; Huang, K.; Shen, D.; Hu, S.; Hensley, M. T.; Caranasos, T. G.; Qian, L.; Cheng, K. *Theranostics* **2018,** 8, 1869-1878.
(46) Zhao, J. Y.; Chen, G.; Gu, Y. P.; Cui, R.; Zhang, Z. L.; Yu, Z. L.; Tang, B.; Zhao, Y. F.; Pang, D. W. *J. Am. Chem. Soc.* **2016,** 138, 1893-1903.
(47) Chen, F.; Ma, M.; Wang, J.; Wang, F.; Chern, S. X.; Zhao, E. R.; Jhunjhunwala, A.; Darmadi, S.; Chen, H.; Jokerst, J. V. *Nanoscale,* **2017,** 9, 402-411.
(48) Busato, A. Bonafede, R. Bontempi, P. Scambi, I. Schiaffino, L. Benati, D. Malatesta, M. Sbarbati, A. Marzola, P. Mariotti, R. *Int. J. Nanomedicine* **2016,** 11, 2481-2490.
(49) Chen, C.; Zong, S.; Wang, Z.; Lu, J.; Zhu, D.; Zhang, Y.; Cui, Y. *ACS Appl. Mater. Interfaces* **2016,** 8, 25825-25833.
(50) Luan, X.; Sansanaphongpricha, K.; Myers, I.; Chen, H.; Yuan, H.; Sun, D. *Acta Pharmacol. Sin.* **2017,** 38, 754-763.
(51) Liu, L.; Sun, C.; Yang, J.; Shi, Y.; Long, Y.; Zheng, H. *Chem-Eur. J.* **2018,** 24, 6148-6154.
(52) Yan, Q.; Chen, Z. H.; Xue, S. F.; Han, X. Y.; Lin, Z. Y.; Zhang, S.; Shi, G.; Zhang, M. *Sensor. Actuat. B: Chem.* **2018,** 268, 108-114.
(53) Liu, S.; Tian, J.; Wang, L.; Sun, X. *Sensor. Actuat. B: Chem.* **2012,** 165, 44-47.
(54) Ni, P.; Sun, Y.; Dai, H.; Hu, J.; Jiang, S.; Wang, Y.; Li, Z. *Biosens. Bioelectron.* **2015,** 63, 47-52.
(55) Guo, Z.; Jia, Y.; Song, X.; Lu, J.; Lu, X.; Liu, B.; Han, J.; Huang, Y.; Zhang, J.; Chen, T. *Anal. Chem.* **2018,** 90, 6124-6130.
(56) Wei, J.; Chang, W.; Qileng, A.; Liu, W.; Zhang, Y.; Rong, S.; Lei, H.; Liu, Y. *Anal. Chem.* **2018,** 90, 9606-9613.
(57) Mayer, M.; Takegami, S.; Neumeier, M.; Rink, S.; Jacobi von Wangelin, A.; Schulte, S.; Vollmer, M.; Griesbeck, A. G.; Duerkop, A.; Baeumner, A. J. *Angew. Chem. Int. Ed.* **2018,** 57, 408-411.
(58) Cao, H.; Wang, Y.; Gao, Y.; Deng, X.; Cong, Y.; Liu, Y.; Jiang X. *Angew. Chem. Int. Ed.* **2019,** 58, 1626-1631.

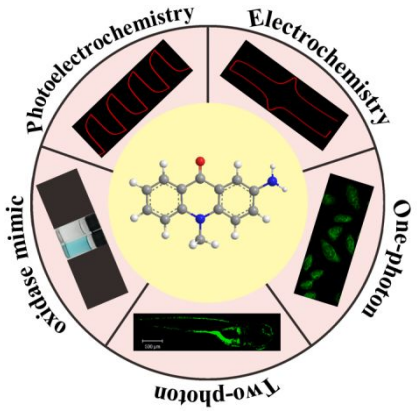

Insert Table of Contents artwork here